electronics

MDPI

Article

On the Design of a Simulation-Assisted Human-Centered Quasi-Stiffness-Based Actuator for Ankle Orthosis

Thomas Mokadim [1,*], Franck Geffard [1] and Bruno Watier [2]

[1] Laboratoire d'Intégration des Systèmes et Technologies, Commissariat à l'Energie Atomique et aux Energies Alternatives, Nano-Innov, Université Paris-Saclay, 91120 Palaiseau, France; franck.geffard@cea.fr
[2] Laboratoire d'Analyse et d'Architecture des Systèmes, Centre National de la Recherche Scientifique—CNRS, Université de Toulouse—UPS, 31000 Toulouse, France; bruno.watier@laas.fr
* Correspondence: thomas.mokadim@cea.fr

Abstract: Most exoskeletons designed to assist users in load-bearing tasks face a mechanical dilemma in their conception. Designers may find a compromise between stiff active actuators-based architectures which are powerful but bulky and compliant actuator-based designs which are much less assistive but less constraining for users. This article presents a new open-source simulation-based design tool and a human-centered method that lets orthosis designers explore different device configurations and evaluate some performance criteria. This framework was applied in three different young-adult subjects. The effects of design personalization on user morphology and gait were studied. First, an ankle–foot orthosis designed to support a 20 kg backpack was defined according to the user's height, weight, and walking speed. Then, a simulation of the subjects fitted with their customized design walking at a self-selected speed on flat ground carrying this additional load was performed. First, the results showed that the designed method inspired by natural joint stiffness behavior provided viable personalized mechanisms. Second, significant reductions in peak joint torque and mean joint activity were observed when comparing muscle-generated torques while the subject was wearing the 20 kg backpack with ankle–foot orthoses on both legs or without. Finally, it shows the value of an open-access tool for exploring the coupling of passive and active actuators to generate lighter and more compliant designs.

Keywords: wearable; robotics; biomechanics; gait analysis; load carrying; OpenSim; MATLAB; Simulink

Citation: Mokadim, T.; Geffard, F.; Watier, B. On the Design of a Simulation-Assisted Human-Centered Quasi-Stiffness-Based Actuator for Ankle Orthosis. *Electronics* **2024**, *13*, 4164. https://doi.org/10.3390/electronics13214164

Academic Editor: Cecilio Angulo

Received: 1 September 2024
Revised: 11 October 2024
Accepted: 15 October 2024
Published: 23 October 2024

1. Introduction

Carrying heavy loads remains a challenge in several tasks, particularly on uneven ground, in industrial contexts, or at home where mechanical help (wheelbarrows, fork lifts, etc.) cannot be used. In this context, exoskeletons could be interesting solutions. Indeed, exoskeletons are a technological possibility that can either be an aid to prevent injuries or bring some strength to the user. Load-carrying exoskeletons have taken different forms in the literature in recent years. The most favored strategy is to develop a full-leg exoskeleton incorporating a structure at back or pelvis level to adapt the load to be carried and, eventually, some remote joint actuators [1–3]. The advantage of this solution is that it directly transfers part of the back load to the ground, to the benefit of the leg. However, these systems require one or more actuators per joint, as well as the corresponding power supply, which can be cumbersome. The user may also experience discomfort when wearing this type of solution, due to the nature of the powerful but rigid electric or hydraulic actuators, which are used in industrial robotics but are not suitable for this application. Finally, to reduce this discomfort, the ankles of these leg exoskeletons are usually left free of powered actuation, such as in the case of the MindWalker exoskeleton [4] or HULC from Lockheed Martin [5].

The other strategy is to assist a single joint with a hip orthosis [6], a knee orthosis [7,8], or an ankle orthosis [9–14]. Despite the lighter weight and lower cost of development of these

solutions compared to a full-leg exoskeleton, the constraints faced by orthosis designers are considerable [15–18]. Orthosis actuators must be adequately actuated to provide the necessary support while limiting additional distal mass and adapt to natural joint kinematics. The system should ensure high autonomy and limit its impact on the user's walking comfort. To borrow the term from telemanipulation, we can speak of maximizing the system's transparency and backdrivability. As walking is a complex, adaptive process, the joints of the leg are constantly adapting their generations of effort and trajectories in order to move the body. This adaptation depends on the walking context, and takes place throughout life. Numerous studies [19–22] show that the ankles are the joints that exert the most important torque and power during the stance phase of ground-level walking.

In [21,23–33], the authors looked at the evolution of ankle quasi-stiffness and its factors of variation. Ankle quasi-stiffness (AQS) refers to the ankle's ability to generate a moment when flexed dorsally or plantarly. This stiffness is expressed in Nm/kg/rad or Nm/kg/deg. This AQS is affected by various parameters such as age [23,24], gender [24], and, mainly, height and weight [27,28,30]. However, within the same subject, the most relevant parameter to study is gait speed [21,24,25,31–33]. Some authors have proposed a model for approximating AQS that takes into account only the subject's height and weight, as in [30]. Others have proposed to reduce the AQS to a set of linear [21,24] and/or non-linear [27–29] springs, whose stiffnesses vary with gait speed.

Designers of lower-limb exoskeletons or ankle orthoses who would like to design a walking aid based on ankle effort assistance have realized that the challenge lies, above all, in the energy compactness of this joint, which is capable of generating on average 1.2 to 1.5 Nm/kg (i.e., ∼100 Nm for a healthy adult) thanks to a few muscles and tendons in a limited volume [15,16,22]. Overcoming these challenges to assist the ankle in generating torque should result in significant, helpful energy savings for the user [22,34].

Solutions explored a few decades ago focused on hydraulic or pneumatic actuators (including pneumatic artificial muscles). Despite their ability to deliver high levels of power when required, the very nature of these actuators limited their mobility. This is less true today; this technology has evolved and is still used (e.g., the HULC exoskeleton, a modern ready-to-use military load-carrying full-leg hydraulic exoskeleton [5]), but the trend today is towards the implementation of fully electric solutions, thanks to advances in portable batteries and electric actuation technology. However, full electric motor-based designs usually weigh too much to feel practical for users for distal joint assistance.

In the literature of recent years, to optimize device behavior, we have seen that compliant actuators are an ongoing trend in exoskeleton and orthosis design, as suggested by study [35]. With a view to reducing the weight and energy consumption of these solutions, passive solutions are being integrated into orthoses to combine compliance, energy storage and restitution, and a reduction in the size of active actuators. In the literature of recent years, to optimize the behavior, we have seen authors integrating electric actuators with fixed-stiffness elastic parts attached in series (series elastic actuators, SEAs) [4,7,36–41] or parallel (parallel electric actuators, PEAs) [36,42], and other actuators with variable-stiffness parts added with lots of different architectures (variable-stiffness actuators, VSAs) [43–53]. According to the authors, these three types of actuators appear to be more suitable in terms of comfort, adaptability, and mass reduction than purely active solutions. Building on the work in [10], some of the same authors have demonstrated that the use of an SEA and a unidirectional PEA (following the recommendations of [54]) together with the appropriate controller in the development of a prosthetic foot [15] provides assistance that is closer to the behavior of a biological foot. Similarly, the subjects who tested this SEA-PEA prosthesis were more likely to wear it than current passive solutions, perceiving less discomfort in their gait. The performance of this prosthetic foot was very similar to that of a biological foot in terms of compactness, weight, and power. This was achieved by breaking down the quasi-ankle stiffness into simplified linear signals, then transposing these signals into technological components [36]. This approach, based on the study of human biomechanics, seems to have been increasingly used in recent years in the design of orthoses and

exoskeletons given the number of published biomechanical studies involving simulations of human-assistive device interaction, e.g., [55], or gait analyses with a view to exploiting the results for the design of assistive devices [56–58]. In [57], the authors propose a method using OpenSim 3.3 open-source software—for which they are part developers—to study the dynamics of a body in motion in order to best size the mechanical components of a customized exoskeleton to assist walking under load. In [55], the authors present their approach to developing a closed-loop simulation of an active knee orthosis coupled to a human subject, in order to test different brace servo strategies. This simulation uses OpenSim® 4.2 for biomechanical simulation, Simulink 2019 for servo-control of the orthosis, and MATLAB 2019 as a pipeline between the tools. This article lays the foundations for a functional tool suitable for exoskeleton and orthosis design. Unfortunately, with the complete overhaul of the OpenSim API in 2021, this tool is no longer usable today. The aim of our study is to develop methods and tools for building a solution and assessing its value in terms of joint assistance when executing a task (e.g., walking and carrying a backpack), taking into account the torque and spacial constraints applying to the ankle orthosis. The first hypothesis is that the ideal solution to assist a joint during load-bearing walks should be personalized to the wearer anatomical needs. It should also limit discomfort in the kinematics of walking, providing assistance only when needed, and reduce the feeling of insecurity and discomfort when wearing a walking device. In a few words, the notions of system transparency and "quasi joint stiffness" such as AQS are essential to the design.

Our work first focuses on the design of an ankle orthosis rather than an orthosis for the other leg joints because the challenge of designing an effective and comfortable load-carrying ankle orthosis still remains for exoskeletons. Through these tools, we design a mechanism that provides the necessary moment to support the ankle torque generation when the foot is on the ground and is as transparent as possible when the foot is in the air and not supporting the body weight. We think it is fair to assume that a bio-inspired design method used to generate actuators and controls for prostheses will perform better than designs integrating standard robotic actuators and focusing on their actuator control strategy. In this context, we ask whether it is possible to optimize the torque generation of an orthosis through its design, or the joints of a leg exoskeleton based on the force response of human joints. We first use existing open tools, then develop new ones and present them here for the community.

2. Materials and Methods

The experimental data used in this study were obtained from an experiment led by Liu et al. [59]. Details of the data acquisition protocol can be checked in this article. The use of OpenSim 4.2 software was also proposed to exploit some of these data and to present our own simulation. For our experiment, only the "GIL06", "GIL08", and "GIL11" subjects were retained, along with their kinematics and the ground reaction forces and moments (GRFMs) associated with their "Free" and "Slow" series. Other subjects in the group were either too young or did not show similarities with the other subjects compared. GIL11 was found to have age, height, weight, and free walking speed characteristics close to those of an average young adult and was considered as the reference subject of our study. GIL06 and GIL08 were found to have almost the same characteristics as GIL11, except for the fact that GIL08 was 9 cm taller than GIL11, and GIL06 weighed 20 kg more than GIL11. The free and slow walking speeds of all subjects were found to be close.

2.1. Biomechanical Models

The OpenSim 4.2 software is provided with several default anatomical and muscular models that have been tested in previous publications [60]. The data of interest in this study concern only walking experiments in the sagittal plane.

2.1.1. Models from Dataset

For this purpose, the OpenSim 4.2 Gait10DOF18musc model was chosen. Details and settings of this model can be found in [61]. This armless model is fitted with 10 DOFs (3 translations at the pelvis; in the saggital plane, 1 pin joint between the pelvis and the trunk–head core; and 1 pin joint for each hip, knee, and ankle joint) and 18 muscles. It shows only the degrees of freedom and muscles required to reproduce gaits recorded in the same sagittal plane. A physical presentation of that model is displayed in Figure 1. The "Scaling" function available in OpenSim was used to scale the default model and create new ones to the proportions of the 3 retained subjects. This was achieved using the scaling tool configuration files.

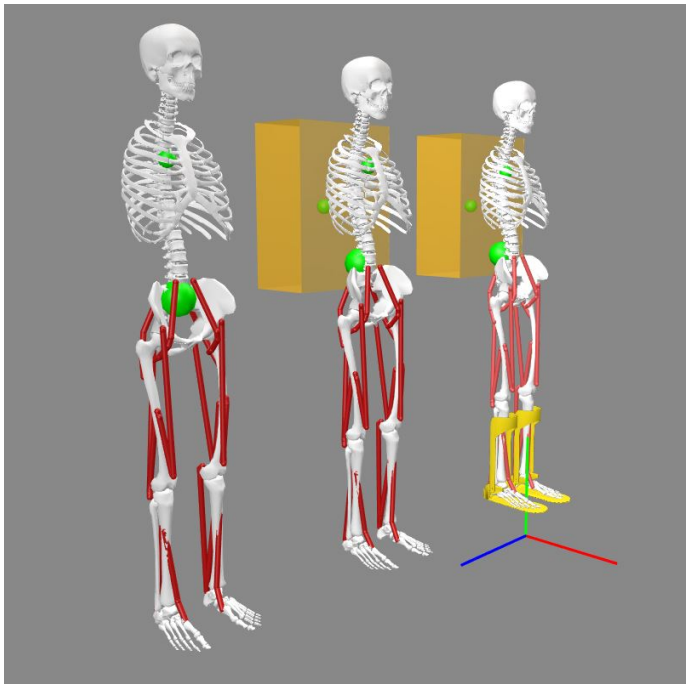

Figure 1. GUI displays of Gait10DOF18Musc models from OpenSim 4.2. From left to right: the original model, the backpack-fitted model, and the double AFO and backpack model. Small green dots display the local mass centers of the torso part, and the backpack if present. Bigger green dots display the global center of mass of the models. One can notice that the augmented models show an upward-and-backward-shifted global center of mass.

2.1.2. Augmented Models

In order to compare the generation of joint muscular effort, particularly that of the ankle, two new types of model were derived from the original one and can be seen in Figure 1. Firstly, the biomechanical model of each subject was augmented with an additional 20 kg backpack load, represented by a plain parallelepiped solid with inertial parameters (Ixx = 2.67 | Iyy = 3.33 | Izz = 1.73 N/mm²). The new solid was welded onto the torso of the biomechanical model at −0.2 m in the fore-aft direction and 0.2 m in the vertical direction from the thorax center of mass. Those two lengths corresponded to an experimental distance measure between the torso barycenter and the 54 × 40 × 22 cm basic backpack worn by the GIL11 model. Eventually, the characteristics and fitting of this extra load onto the basic model could be customized. Secondly, a new model was featured with a two-part ankle–foot orthosis (AFO) on each leg. The AFOs had non-zero mass and inertial parameters, but they were low enough (100 g per piece, Ixx = 5.0×10^{-3} | Iyy = 1.25×10^{-2} | Izz = 1.4×10^{-2} N/mm²) not to impact the model. If required, one is free to modify these parameters to simulate a particular design. The upper and lower parts of the AFOs are linked by a pin joint. As OpenSim 4.2 does not support closed kinematic chains, AFO parts are linked to the tibia and talus bones by bushing forces on each leg. These forces act like spring-damper constraints applied between reference frames attached to their respective bodies. A virtual

controller-based massless torque generator is declared on the pin joint of the AFOs. The AFOs are positioned so that their axis of rotation coincides with the model's simplified pin joint ankle axis of rotation in the sagittal plane and bushing forces are set to transmit torques between the AFO and the foot while keeping the AFO in place. Inspired by the backpack implementation, a localized actuator of known mass can be declared for the model for further research.

2.2. Simulations Workflows

The three next sections will explain how to use the framework according to each experimental condition. Figure 2 will help the reader to locate which feature is put to use.

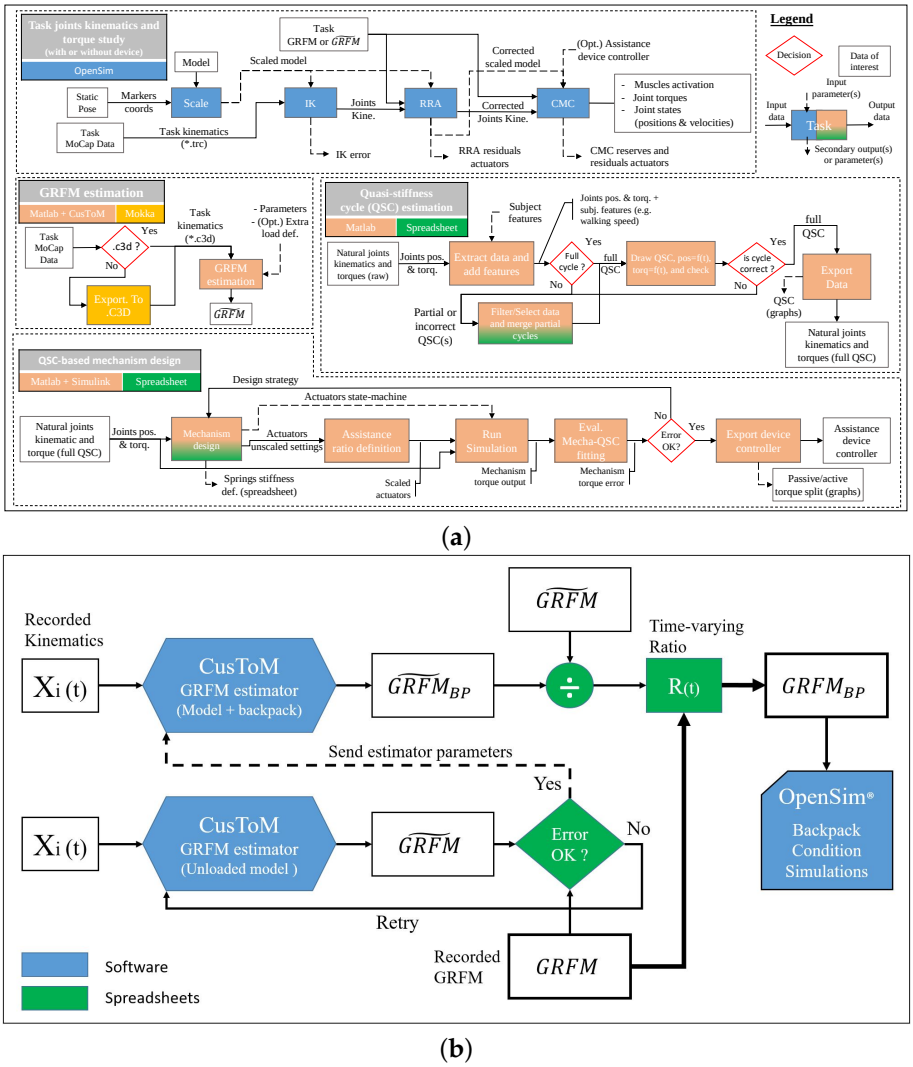

(**a**)

(**b**)

Figure 2. Framework workflow and GRFM estimation method diagram used in this paper. (**a**) Diagram of the entire framework, available at https://github.com/MokaMech/HJOSET (accessed on 10 august 2024). Main features are, from top to bottom: the muscle and dynamic task study through the OpenSim 4.2 tool pipeline; the GRFM estimation and quasi-stiffness cycle estimation for AQS though MATLAB; and the Simulink-based mechanism design tool that serves as a device controller generator for the OpenSim CMC tool. (**b**) Flowchart of the workflow used to estimate the GRFMs of the added 20 kg backpack from the original recorded GRFMs. The transformation between the two signals resulted from a time-varying ratio obtained through two CusToM simulation runs with unloaded and backpack-loaded models, respectively. The two simulations ran from the same kinematics and tool parameters. The tilde notation is to represent the estimation aspect of the corresponded data.

2.2.1. No-Load Models

For each subject, the scaled model was used, along with the recorded inverse kinematics and GRFMs. Data were acquired while the subjects were walking on flat ground at several slow (0.70 and 0.81 m/s) and free (1.11, 1.12, and 1.17 m/s) self-selected speeds. The detailed protocol was reported in [62]. OpenSim's Residual Reduction Algorithm (RRA) was used to reduce the residual effort [63]. These came from the aggregate marker data-processing errors which make the model compensate for nonphysical forces. By altering the torso mass center of the subject-specific model, this algorithm permits the kinematics computed from Inverse Kinematics to slightly adjust to be more consistent with the recorded GRFM data. The RRA tool was used twice, as suggested in [57], with the first iteration generating a corrected model with new centers of mass for each body to reduce the residual forces, and the second iteration generating the inverse kinematics that minimize these kinematics reconstruction errors when applied to the corrected model. The second iteration was also used to determine joint torques by means of an inverse dynamics calculation. The final tool in the workflow was OpenSim's 4.2 "Computed Muscle Control" tool [64], which used the corrected model, kinematics, joint torques, and an objective function to determine the forces generated by each of the muscles making up the model's joint muscle torques. With the "Gait10dof18musc" model, the ankle joint torque was derived from the tibial anterior (TA), soleus (SOL), and gastrocnemius (GAS) muscles.

2.2.2. Load-Carrying Models and Data

The major difference compared to the previous experimental condition is that the GRFMs were not derived from the dataset, and OpenSim 4.2 does not provide a feature to estimate GRFMs. Instead, an open-source MATLAB toolbox named CusToM [65] was used. The CusToM toolbox, which is designed for biomechanical modeling and is based on the MATLAB environment and several other MATLAB toolboxes, was used to estimate the ground reaction forces and moments (GRFMs) for each subject in the dataset and for each walking speed. Figure 2b illustrates the workflow described below to estimate the loaded GRFMs.

First, an equivalent biomechanical model was defined for each subject using the raw positions of the motion capture markers *Xi* (see .c3d files) and the model and tool parameters. Inverse kinematics and inverse dynamics were then calculated, and a GRFM estimate—$\widetilde{GRFM}$—was prescribed. The difference between the estimated GRFMs and the recorded GRFMs was then evaluated.

As the peaks and trends of the estimated GRFMs matched those of the recorded GRFMs, a second estimate was made using the same tool parameters and model but with the addition of a 20 kg backpack, similar to the augmented models in OpenSim 4.2. To create this new model, a snippet of code was inserted into the main function of CusToM to compute a new mass and center of mass for the thorax in the biomechanical model generated by the toolbox before estimating the inverse dynamics and GRFMs. Both GRFMs were then visualized in a spreadsheet with graphics, and the estimated GRFMs with the backpack—$\widetilde{GRFM}_{BP}$—was deconvolved with the estimated GRFMs without the backpack $\widetilde{GRFM}$. The result was the time-varying ratio signal *R(t)* between the two GRFMs. This ratio was then applied to the recorded unloaded data *GRFMs*, which matched the dataset kinematics better, to obtain an estimate as if they had been equipped with a 20 kg backpack—called $GRFM_{BP}$. Since the estimated GRFMs were obtained, the same steps as for the no-load simulations were repeated with the new data.

Validation of the GRFM estimation method: To evaluate the accuracy of the new GRFM data, an error threshold based on the model weight was established. This threshold was set to 5%, as described in [66], to determine if the signal was "good enough" for our simulation. In addition, a visual examination of the induced center of pressure and vector component of the new GRFMs was conducted to ensure that they behaved in the same manner as the original GRFMs. Specifically, we checked that the center of pressure

appeared at the same location and moved in the same direction under the feet, and that the new GRFM vector originated from this new center of pressure and pointed towards the corrected center of mass of the backpacked model. Based on these assessments, we concluded that the new GRFMs estimated by this transformation method were sufficiently accurate for our simulation.

2.2.3. AFO-Equipped Load-Carrying Models

In this model, which included both unloaded and loaded conditions with a 20 kg backpack and AFOs on both legs, OpenSim's CMC tool was used to determine the forces generated by the muscles, taking into account any device assistance described in the torque constraints file. The assistance profile was designed using a MATLAB/Simulink simulation based on the weight-normalized joint muscle torque-generation profile as a function of ankle position, as shown in [36]. These curves are referred to as AQS curves earlier in this article. Using the RRA kinematics and joint torque results obtained in the unloaded condition experiment, we plotted the AQS curves for each subject. These curves were then used to hypothesize mechanisms of generation by manually approximating them using passive and active components such as linear torsional springs and electric actuators (see Figure 3).

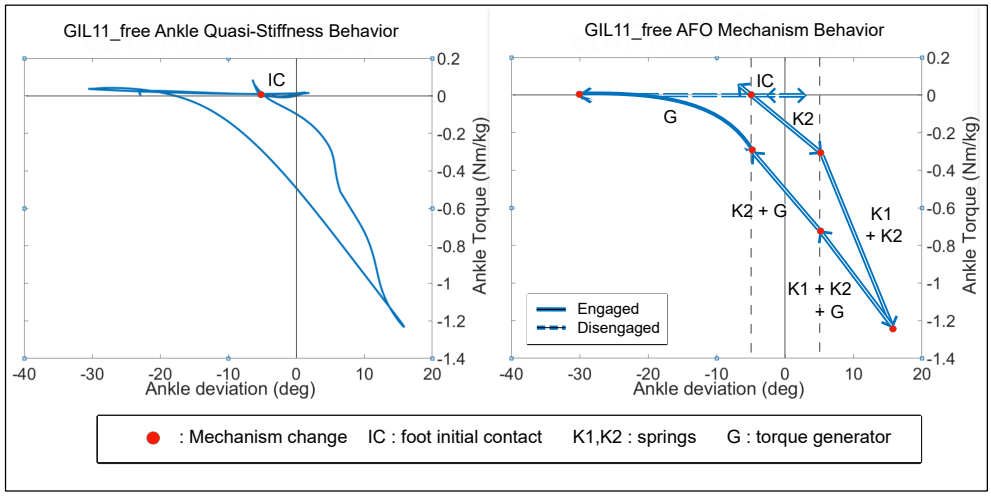

Figure 3. Example of fitting of the reference subject GIL11 AQS profile (female, 18 years old, 63.1 kg, 1.63 m) at free speed (1.17 m/s). Reference profile is displayed on the left. Mechanism generation is displayed on the right. It is composed of two linear springs (*K1*, *K2*) and an external torque generator (*G*). The starting point at the left leg initial contact (IC) is pointed out by a red dot on the two curves. The AFO torque profile evolved following the arrow marks. During the swing phase (from −30° to IC clockwise), no component was enabled. Other mechanism designs can be found in Appendix A.

The Simulink project was based on a workflow that simulates a virtual mechanism designed to implement a personalized actuation strategy. The mechanism is defined using the components chosen from the breakdown of the subject-related AQS curves, and can be modified to fit the strategy to be implemented.

The Simulink project takes as input the kinematics and joint torques calculated by the RRA tool for the subject and load case under consideration. The stiffness of passive mechanical components is defined in Nm/kg/deg and the stiffness of active components in Nm/kg. The assistance torque provided by the active actuators and the product of passive stiffness and ankle deviation is called "unscaled assistance" and its unit is Nm/kg. A scaling factor in kg is applied to each component's output to fit the mass the device is supposed to balance. The scaling factor can be adjusted to fit the design and determine the torque characteristics of the components implemented in the mechanism, which will be used for the implementation of the actuation strategy during prototyping.

The subject-specific weight-normalized torque-generation behavior of the active and passive components during simulation is compared with its AQS curve, and the RMS error is computed between both torque-generation profiles. To achieve this torque-generation behavior, we implemented two parallel linear springs and a torque generator in the mechanism. Springs are represented according to their stiffness and their operating range (depending on the ankle angle deviation, and on the gait phase for which they are intended). The torque generator is represented by its nominal maximum torque, based on the maximum difference between natural ankle joint torque and the torque provided by the springs identified by the simulation. The torque generator and springs are considered as actuated and separated, with no assumption of their body attachment. Regarding the desired assistance strategy, one is free to implement any kind of component or change the preset mechanism. The default mechanism design implements a PEA with two parallel springs and an electric motor. Once the mechanism satisfies all design constraints and objectives, the forces generated during simulation of the mechanism and scaled by the assistance scaling factor are pasted into a file that can be interpreted by OpenSim 4.2 as a constraint file driving the orthoses of the AFO-augmented model. The AFO models can then be edited to integrate the retained components according to the simulation findings.

The experiment workflow concludes by running the OpenSim tools pipeline one last time on the AFO- and backpack-augmented model. The CMC tool is used to determine the joint muscle torque generated by the TA, SOL, and GAS muscles of each leg, assisted by the strategy simulated in the Simulink project. The muscles' generated torque is compared with the RRA results from the unassisted load-bearing and no-load cases to assess the differences in joint muscle torque generation.

From that point, performance metrics can be computed to evaluate the potential of the estimated assistance strategies.

3. Results

3.1. AQS Profile Breakdowns

The workflow described above enabled us to create personalized assistance profiles for each subject and their respective free and slow walking speeds. The resulting mechanism was designed to systematically break down the AQS curves into passive and active actuators, regardless of the subject or speed being considered.

3.1.1. Passive Assistance

Figure 3 shows an example of the breakdown of GIL11's free AQS profile into a personalized AFO mechanism, illustrating the output of the method proposed in this study. This analysis was also performed for the other cases, which can be found in Appendix A.

To provide assistance to the user at the correct time, the *K2* spring in the personalized AFO mechanism needs to be triggered at the moment of initial contact (IC) between the foot and the ground, as indicated by the red dot in Figure 3. The timing of this initial trigger varied for each subject. For example, in the case of GIL11 at free speed, the IC event occurred when the ankle deviation reached -5.0 degrees.

Following the IC event, the load is transferred onto the user's stance leg as they move forward. During this phase of the gait cycle, the *K2* spring is engaged and stores potential energy, which is then released to provide assistance. The working range of the *K2* spring is subject specific and, in the case of GIL11, it was triggered from $-5.0°$ to $-6.5°$, corresponding to the foot flat gait event, up to 15.0°.

In the proposed AFO mechanisms, an additional spring, *K1*, is included to better match the non-linear load response of the AQS curve during the gait phase. The stiffness of *K1* is several times higher than that of *K2* and is triggered after *K2*.

The working ranges of the springs and their corresponding angular stiffness values for each study case can be found in Table 1.

Table 1. Summary of mechanism characteristics for each subject and speed. The mechanisms have been sized to relieve 20 kg from the user. User weights are expressed free of extra load. This table lists all angular stiffness and engagement ranges for the *K1* and *K2* springs. The maximal torques supplied by *G* in each condition are also listed. RMS errors (in Nm/kg) were computed between the raw unscaled mechanism resulting from the AQS breakdown and the reference torque delivered by the AQS profile over time.

Subjects	Speeds (m/s)	K2 Spring				K1 Spring			Torque Gen.	RMSE Error of Unscaled Assistance (Nm/kg)
		Angular Stiffness (Nm/deg)	Working Range (deg)			Angular Stiffness (Nm/deg)	Working Range (deg)		Max Torque (Nm)	
			Min	Trigger	Max		from	to		
G6 (1.57 m, 81.9 kg)	1.11	2.87	−7.0	−4.0	12.5	7.37	2.5	12.5	13.0	0.0221
	0.81	3.11	−10.0	−8.0	8.0	5.32	−1.6	8.0	6.3	0.1004
G8 (1.72 m, 61.9 kg)	1.12	0.93	−5.0	−1.2	17.0	8.36	7.0	17.0	16.0	0.0136
	0.7	1.11	−5.0	−0.5	16.0	8.36	7.5	16.0	10.5	0.0112
G11 (1.63 m, 63.1 kg)	1.17	1.78	−6.5	−5.0	15.0	4.10	5.0	15.0	9.4	0.0375
	0.8	2.46	−12.0	−8.0	13.0	6.06	8.0	13.0	4.1	0.0418

3.1.2. Active Assistance

The active element of the mechanism is triggered when necessary, based on the breakdown of the AQS curve for each subject and speed. The actuation profile for the active element, denoted as *G*, is determined to minimize the error between the subject's AQS curve and the torque generated by the AFO.

As shown in the example in Figure 3, the torque generator *G* is triggered during the hysteresis feedback loop, either alone or in combination with the passive actuators *K1* and *K2*. The maximum required torque for the active component in each condition is also reported in Table 1. The full breakdown of the AQS curves for the passive actuators can be found in Appendix A.

3.1.3. RMS Fitting Error

For each condition, an RMS error was computed between the unscaled assistance torque generated by the personalized mechanism and the subject's AQS torque over the time simulation, which equals the elapsed time over one stride. The mean RMSE across all mechanisms was 0.0377 ± 0.033 Nm/kg. RMS values ranged from 0.1004 for GIL06 at slow speed to 0.0112 for GIL08 at slow speed.

RMS values for other conditions can be found in Table 1.

3.2. Device Performance Evaluation

For each subject and walking speed, the OpenSim 4.2 RRA right and left ankle torque results for both unloaded and load-carrying conditions are plotted against the simulation time in Figure 4. Additionally, the OpenSim CMC right and left ankle torque results generated by the sum of the soleus (SOL), gastrocnemius (GAS), and tibialis anterior (TA) muscles during the AFO-braced load-carrying conditions are also plotted against their respective simulation times in the same figure. It is important to note that the negative torque values observable in the plots are solely due to the frame orientation in the OpenSim simulation.

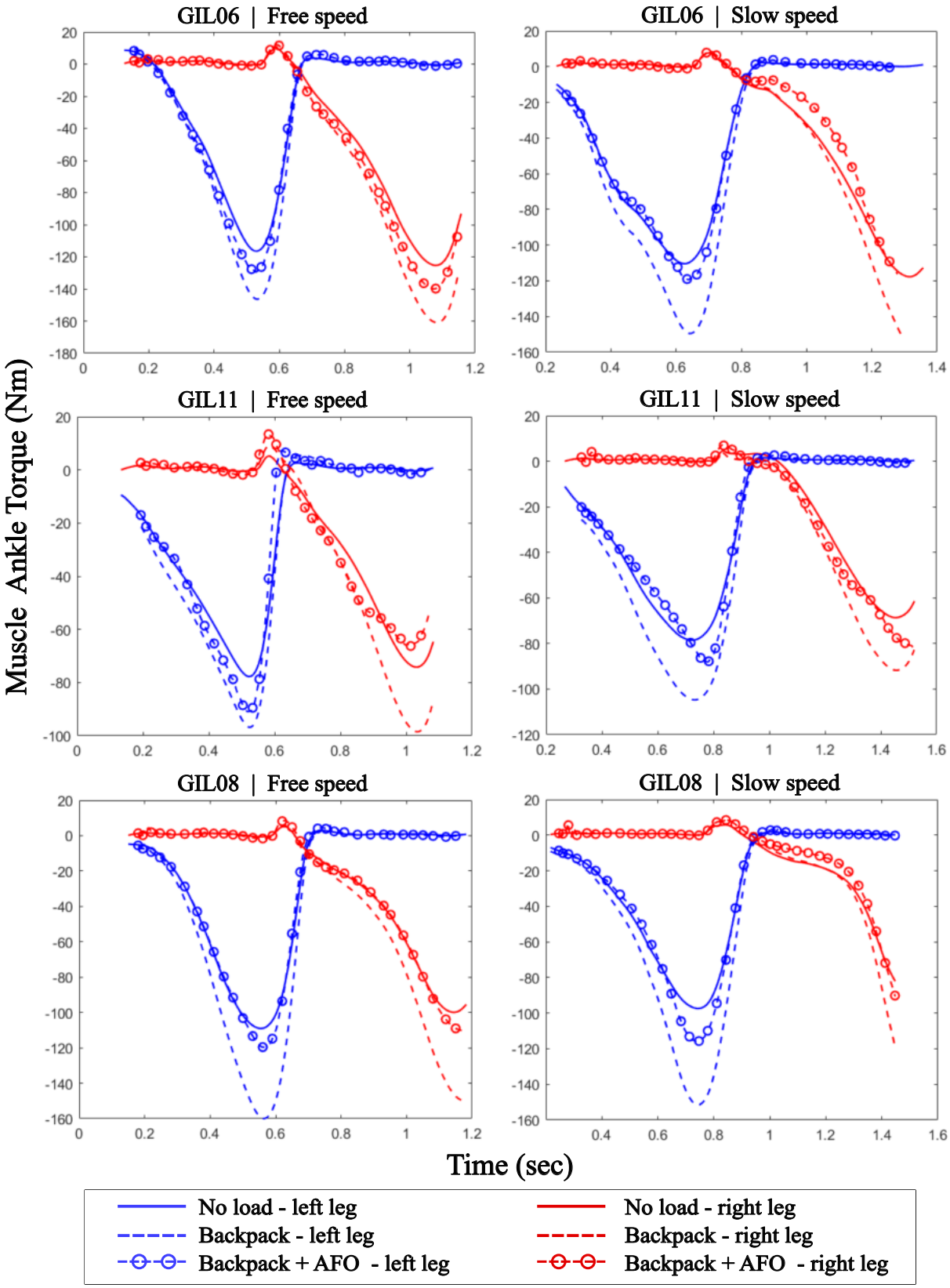

Figure 4. Right and left leg torque generation of each subject under each load condition at free and slow speeds. This plot displays the RRA torque output of the unloaded (full line) and backpack-carrying (dashed line) conditions against time. The torque generated by the contraction of the SOL, GAS, and TA muscles (circled dashed line) is also plotted against time. Refer to Table 2 for evaluation metrics.

Table 2. Summary of the evaluation metrics of right and left leg AFO mechanisms for each subject carrying the 20 kg backpack. User weights are expressed free of extra load. Refer to Figure 2 for time visualization of the provided assistance.

Subjects	Speeds (m/s)	Peak Torques Difference						Mean Activity Saving (%)		
		Left Leg		Right Leg		Mean		Left Leg	Right Leg	Mean
		(Nm)	(%)	(Nm)	(%)	(Nm)	(%)			
G6	free	16.79	−11.47	21.08	−13.09	18.93	−12.28	−12.52	−12.43	−12.47
	slow	30.00	−20.06	33.73	−22.48	31.86	−21.27	−17.47	−21.70	−19.58
G8	free	40.23	−25.15	41.00	−27.08	40.62	−26.12	−22.62	−18.03	−20.33
	slow	35.25	−23.27	28.74	−24.08	31.99	−23.67	−18.49	−22.96	−20.73
G11	free	5.86	−6.06	32.03	−32.52	18.95	−19.29	−15.09	−15.42	−15.26
	slow	16.53	−15.78	9.06	−9.87	12.79	−12.83	−19.23	−13.21	−16.22

3.2.1. Ankle Muscle Peak Torque

Figure 4 highlights the increased torque demand on the ankles when the subjects were carrying a 20 kg backpack and walking at the same speed as in unloaded conditions. The major difference in the torque request occurred during the power plantar flexion event, where the torque curves peaked.

In all conditions, wearing subject-specific AFOs on both legs helped the subjects to reduce the mean peak torque request to transport the load, with a mean value of around $-19.24 \pm 5.6676\%$. It is worth noting that, in the GIL06 and GIL08 cases at slow speed, where the subjects were wearing a backpack and an AFO on the right leg, the designed mechanism allowed the users to output less torque during the early load transfer phase than that requested in the unloaded condition. The values of this reduction for each condition can be found in Table 2.

3.2.2. Ankle Muscle Activity

The way the assistance was supplied is also noticeable in Figure 4. One can notice that the reduction in the requested torque in the third condition is pretty well distributed across the duration of the simulation. The more the gap between the torques requested by the models in the first and second conditions widened, the more the assistance provided by the AFO was noticeable, making the muscle ankle torque curve of the third condition try to stick to the unloaded condition curves. The mean reduction in muscle ankle torques requested during the second and third conditions across all subjects on both legs was about $-17.43 \pm 3.31\%$. The maximum reduction occurred for GIL08 at slow speed, -20.73%, whereas the minimum saving was attributed to GIL06 at free speed, -12.47%. Every value of the reduction for each subject and condition can be found in Table 2.

4. Discussion

This paper presented a human-centered orthosis design methodology. This method has been explored as an aid for the design of task- and user-specific devices. Defining a configurable framework to evaluate this approach was the main objective. The second one was to assess if this tool outputted technically viable, and eventually personalized, solutions. As far as we can say, from this work, these two objectives have been reached, since the presented framework allows designers to explore different assistance strategies and their realizations according to a set of constraints given a certain task. Thanks to this tool, a bio-inspired design of an AFO has been reproduced with similar assistive components to those seen in [15]. Moreover, a similar approach could be applied to other joints.

4.1. Results Interpretation

Using the tool presented in Section 2.2, the effects of an ankle orthosis were determined for the reference user GIL11. The effects of variations in walking speed on the ideal orthosis

assistance profile were also studied. In addition, the selection of other users walking at similar speeds but with different height and weight characteristics allowed us to compare the impact of these three parameters—height, total weight, and walking speed—on their gait pattern and the associated ankle quasi-stiffness.

In all these cases, the assistance provided by AFOs sized to relieve 20 kg of the user's weight, corresponding to the weight of the backpack, made the user achieve a significant saving in joint torque. This saving was all the more notable for GIL06 at slow speed and for GIL08 at slow and free speeds since it was close to a 20% saving. This value is encouraging, as the AFO-declared mass is only 200 g, and thus it leads us to think that remotely actuated AFOs which are lighter than in situ actuated ones should bring better assistance to the ankle joint.

When AFOs were worn by subjects GIL06 and GIL11 at slow speeds, as well as GIL08, under load-bearing conditions, it was possible for them to achieve a muscular effort almost similar to that in the unloaded case during walking, except in the vicinity of plantar flexion, where the work of the joint is greatest. In some rare cases, the assistance provided by the AFOs overrode the weight shift and saved more torque than necessary, allowing the wearer to exert less joint torque than in the unloaded condition.

The AFO's assistance to the user during walking was based on their gait profiles in unloaded conditions, taking into account a walking speed independent of the additional weight. This approach allowed for the AFO's power to be sized in a scalable fashion based on the mass to be relieved. Passive elements such as springs were found to be ideally suited to this challenge. The method presented in this study highlights the fact that the use of an active torque generator is only necessary if the contribution of passive elements is insufficient. By providing only the missing work between the reference and the spring-based torque, the power required by the torque generator could be reduced.

For example, in the case of GIL11 at normal speed, a Maxon(Sachseln, Switzerland) RE50 200 W motor [67] and GP52 gearbox (53:1), with a total weight of 1.870 kg, could relieve 20 kg from the subject using a 24 Nm torque generator. The AQS breakdown method suggested the same task could be achieved with an RE40 150 W motor and its GP42 (53:1) gearbox from the same manufacturer, delivering a maximum torque of 10.1 Nm, paired with two compression springs, K1 [68] and K2 [69], and lever arms compact enough to be implemented in the mechanism (respective stiffness, lever length, and mass are K1 = 3.14 daN/mm, L1 = 50 mm, and m1 = 0.024 kg | K2 = 8.7 daN/mm, L2 = 80 mm, m2 = 0.049 kg) Spring references are taken from the Vanel(Birkirkara, Malta) manufacturer catalog. The new total actuator mass weight is 1.013 kg, i.e., 46% less than the previous solution.

The proposed method in this study involves the identification and simulation of a mechanism based on the subjects' AQS profiles, with the aim of fitting as closely as possible to their support needs while also respecting the designer's constraints. The root mean square (RMS) error observed for each mechanism generation was acceptable, with a value of less than 0.05, except for in the case of GIL08 at slow speed. In this particular case, the error slightly exceeded the value of 0.1, which may be attributed to the fact that the design of the mechanism allowed for a result that exceeded the simple compensation of 20 kg on the right leg, resulting in a greater error compared with the reference signal.

The results obtained using the proposed method in this study should be compared with those presented in [15]. The authors of that study also chose to implement two springs of different stiffness and an electric torque generator in their prostheses, with the characteristics and roles of these elements in the mechanism identified using AQS curves. The GIL11 gait pattern at free speed used in this study was similar to the 'generic' case walking at a speed of 1.25 m/s used by the authors to identify their system. The results of our method showed similarities in the behavior and roles of the selected actuators when implementing the mechanism as compared to the results presented in [15]. However, our results also indicated that, for the same individual, different walking speeds could result in different mechanisms, with variations in the use of actuators and their characteristics. Table 1 shows that the intra-personal variation in the stiffness of the passive mechanical

elements was not negligible, but was less than the interpersonal variation. Additionally, the operating range of the passive elements and the maximum torque required by the motor could also vary within the same individual, depending on their walking speed, and between individuals, based on their morphology.

Some authors, such as those of [27], suggest that the quasi-stiffness of the ankle between the ground contact phase and power plantar flexion is non-linear. Our observation of the AQS curves also supported this trend, and our method assumes that such stiffness can be implemented in the design of the AFO. As a result, the design of the AFO is likely to be more complex, integrating several passive elements with linear stiffness, as well as a motor. However, the use of simulation in conjunction with this method of exploring assistance design allows for the testing of different architectures, such as a simpler mechanism with just one non-linear spring or two linear springs. This approach enables a compromise between performance and simplicity to be explored.

If the designer wishes to develop a solution able to assist the three subjects of this study with a single mechanism while trying to retain the personalized nature of the assistance, VSAs might be an appropriate concept to consider. Nevertheless, the multitude of possible designs for VSAs, as illustrated by the state of the art, show that defining an ideal solution is no easy task. Even though the authors of these articles, such as [43], clearly indicated that they were dedicating their VSA to an orthosis and their embedded constraints at the end of a limb, the weight and torque delivered by these prototypes did not live up to their expectations.

It is important to note that torque efficiency with respect to a reference is not the sole objective to be pursued by designers. As illustrated by the GIL11 case study, reducing mass is also a crucial objective in enhancing device wearability. It is important to note that added masses can significantly impact the subject's gait and posture. In their study, Vijayan et al. [70] found that adding up to 1.13 kg, 2.5 kg, and 7.25 kg around the ankle joint, knee joint, and pelvis, respectively, did not significantly impede gait in young and healthy subjects. These findings could be considered useful guidelines that complement our work.

Using this tool and the proposed design method, the designer can explore the quasi-stiffness of one or more joints, which refers to the generation of joint effort required to achieve a reference trajectory for a specific task, such as loaded walking. In [58], the authors presented another application of OpenSim 4.0 software for designing orthoses or exoskeletons based on the results of inverse dynamics from motion capture data, which may be a quick and cost-effective way to size the device assistance needs. It is also worth using OpenSim's CMC tool, as in [57,59], where ideal joint assistance is defined to explore its characteristics. However, our tool is unique in that it provides an open-loop system for the identification, design, and parameterization of the mechanical behavior and desired controls of the assistance in great detail during the design phase. In fact, it uses the MATLAB/Simulink template project to provide guides and tools for configuring the assistance according to the torque profiles to be achieved. In this way, the internal division between passive and active actuators enables a detailed analysis of assistance for the two types of actuation. Combined with OpenSim AFO and/or backpack custom models, designers can test and evaluate their system architecture in the OpenSim environment. Following the initial execution of the framework to ascertain the optimal mechanical design from the subject, it is advised to undertake a second run of the workflow with more comprehensive modeled components attached to OpenSim biomechanical models. This approach, particularly the incorporation of added mass distribution in close proximity to the desired prototype, is instrumental in refining the forecasted outcomes. We gave the HULC and Mindwalker examples in introduction as efficient yet passive ankle joint lower-limb exoskeletons. The proposed methodology can be effectively applied to existing lower-limb assistance devices by fitting them onto a default model. This allows for the exploration of mechanism variants or the addition of actuation for other joints, which can then be evaluated in terms of the resulting new incomes. In essence, defining an average

quasi-passive ankle joint mechanism using this framework would facilitate further weight reduction and enhance gait energy efficiency ([57], Figure 1). To our knowledge, no other up-to-date open-source software provides this kind of end-to-end design support.

4.2. Study Limitations

While the tool presented in this article has several advantages and unique features, it is important to acknowledge its limitations. One such limitation is related to the estimation of ground reaction forces and moments (GRFMs) using the CusToM toolbox. The approximation method used for GRFM estimation instead of the straight application of the CusToM workflow involves a discrepancy in parameterization between the biomechanical models reported in OpenSim 4.2 and those in the CusToM toolbox. Nevertheless, these discrepancies are less than 5% of the load-carrying model weights. As such, it under- or over-evaluates the extra torque generation by up to $\pm$2.5% in the load-bearing case, or the assumed performances of the design when comparing the ankle torque generation between cases 1 and 3. However, it is worth noting that the authors of the CusToM toolbox have published recent papers that attest to the effectiveness of their work in estimating GRFM data [71].

Additionally, the current implementation of the tool only allows for the design of AFOs for a single subject at a time. This may limit its usefulness for researchers or clinicians who need to design assistive devices for multiple subjects in a timely manner. Finally, the tool has only been tested and validated on a limited number of subjects and walking conditions. Further testing and validation on a larger and more diverse population, as well as in different walking scenarios, are necessary to establish the generalizability and robustness of the tool (Figure 4).

The second data-related limitation lies in the difficulty of finding motion capture data for which the exact tread velocities are known, as well as the GFRMs available with the kinematics. The dataset presented in [59] would have been suitable for this work, but, unfortunately, the format and availability of the data made it impossible to exploit today. The only dataset found that could be used was that of [57]. Nevertheless, the recordings did not allow us to study the motion of each leg over a complete stride. As a result, the AQS profiles of each subject resulted from a fusion of part of the kinematics of each leg, including defects with respect to the average gait kinematics of each subject, which may have introduced discrepancies in the sizing of the AFO and therefore in the gait assistance visible in Figure 4.

In addition, an estimation of the reduction in muscle-generated torque induced by wearing an AFO was only provided by this method. This estimation may lack precision compared to ground tests due to the coupling of several simulation results and manual approximation of designs. Despite every precaution being taken to define an elastic coupling between the AFO and the subject's limbs in simulation, the mechanical stresses located at these points during a physical test with a prototype and the dynamic behavior of the mechanical elements are not comparable with the estimated results. To simplify this simulation implementation, user training effects, changes in kinematics and/or walking speeds [70], or unwanted load transfer to another joint [72] due to the assistance were not implemented in this framework as it stands. The conclusions from [72] on gait disturbance while wearing joint devices are relevant and must be kept in mind by orthosis designers. However, these results may be carefully transposed to our work as the AFO design may vary. Attention should also be focused on the way in which OpenSim 4.2 software manages joint-assistance-induced kinematic changes. In [57], the authors showed that assisting ankle plantar flexion with an ideal spring-based AFO involving the same power we used has limited effects on other joints' torque generation in young healthy subjects. Thus, as the authors of [70] concluded in their work on the non-significant change in gait while carrying additional weights from devices on lower limbs up to a limit, we may rightfully suppose the kinematic is still good enough to evaluate assisting strategies with ankle devices defined in similar conditions without impeding other joints. All these aspects have already been partially reported in [57] and should be taken into account when testing

prototypes. Nevertheless, this work can be considered both useful and interesting for the design community, as it is available in an open-access repository and provides access to goal-oriented tools to help designers make choices before they commit to long test and trial cycles.

5. Conclusions

Through this simulation and method, we think we managed to find a way to define a helpful device-generation tool focusing on the subjects. Orthoses designers willing to tackle the issues of personalizing their devices to a specific task and fitting its assistive power to a number of subjects may gain an idea of the pros and cons of their design. They are free to add any plugins or functions that could enhance the possibilities of this work. Future plans for this simulation are to use it to explore different actuation strategies like motor-only- and spring-only-based assistance on flat walking tasks, and eventually other ambulation tasks. The next steps that would be helpful involve coming up with a variable-stiffness actuator presenting advantages and able to configure itself and match a subject's AQS profile as well as possible. A supplementary experiment involving test subjects and a prototype should verify the trends forecasted by the simulation.

Author Contributions: Conceptualization, T.M.; methodology, T.M.; software, T.M.; validation, T.M.; formal analysis, T.M.; investigation, T.M.; resources, T.M. and F.G.; data curation, T.M.; writing—original draft preparation, T.M.; writing—review and editing, T.M., F.G., and B.W.; visualization, T.M.; supervision, B.W.; project administration, F.G.; funding acquisition, F.G. All authors have read and agreed to the published version of the manuscript.

Funding: This research received no external funding.

Data Availability Statement: The original data presented in the study are openly available in the HJOSET repository at https://github.com/MokaMech/HJOSET (accessed on 10 August 2024).

Acknowledgments: The authors would like to thank C. Pontonnier and A. Schuster from Rennes University (France) for having taken the time to troubleshoot our issues using their 'CusToM' MATLAB toolbox.

Conflicts of Interest: The authors declare no conflicts of interest.

Abbreviations

The following abbreviations are used in this manuscript:

AFO	Ankle–Foot Orthosis
AQS	Ankle Quasi-Stiffness
CMC	Computed Muscle Control
GAS	Gastrocnemius Muscle
GRFM	Ground Reaction Forces and Moments
RRA	Residual Reduction Algorithm
SEA	Series Elastic Actuator
SOL	Soleus Muscle
TA	Tibial Anterior Muscle
PEA	Parallel Elastic Actuator
VSA	Variable-Stiffness Actuator

Appendix A. Subjects' AFO Torque-Generation Profiles

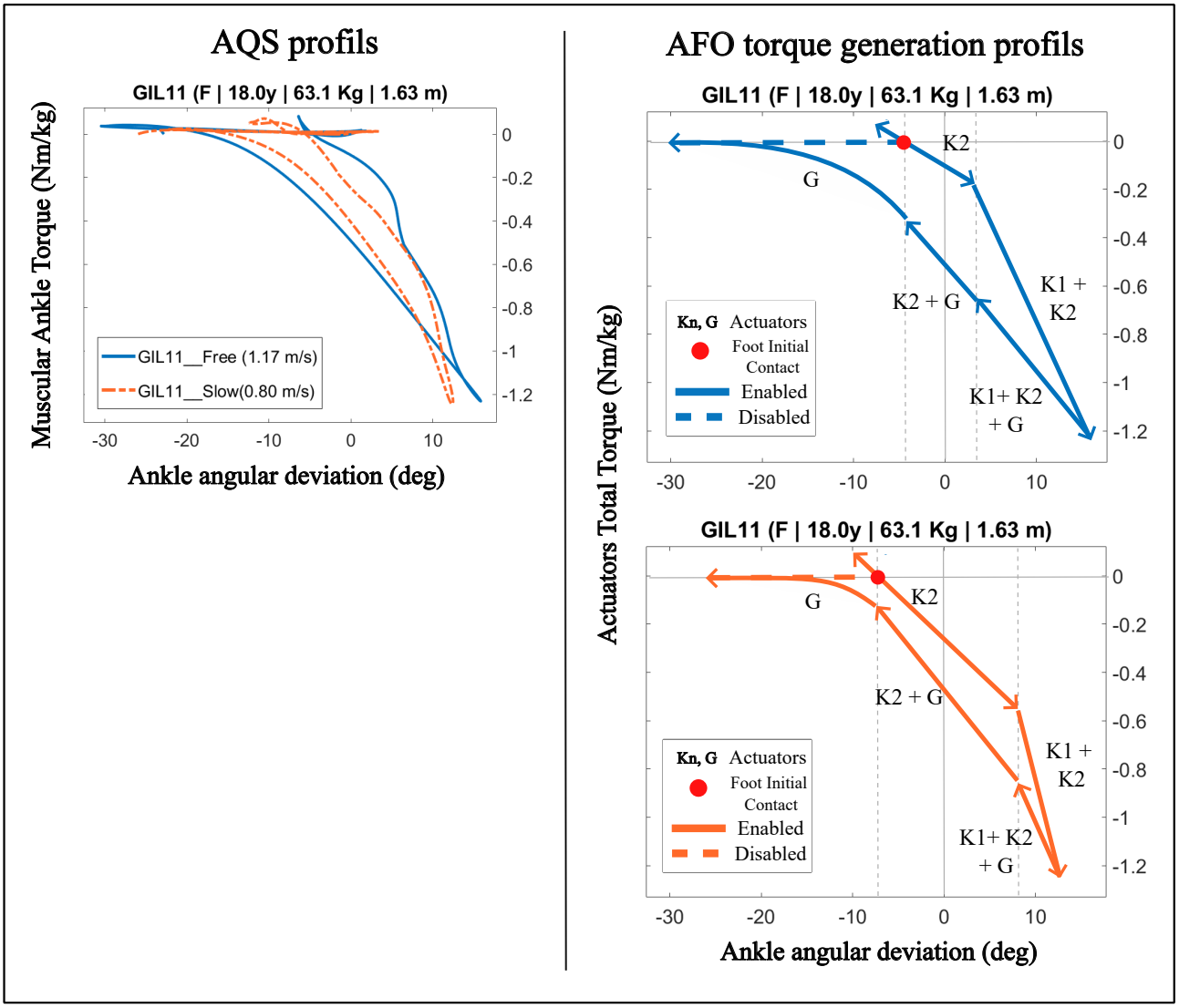

Figure A1. Fitting of the original AQS of reference subject GIL11 (female, 18 years old, 63.1 kg, 1.63 m) at free and slow speeds (1.17 and 0.80 m/s) with linear springs (*K1*, *K2*) and an external torque generator (*G*). The starting point at the left leg initial contact is pointed out by a red dot on the 2 rights curves. The AFO torque profile evolved following the arrow marks. During the swing phase (from −30° to IC clockwise), no component was enabled.

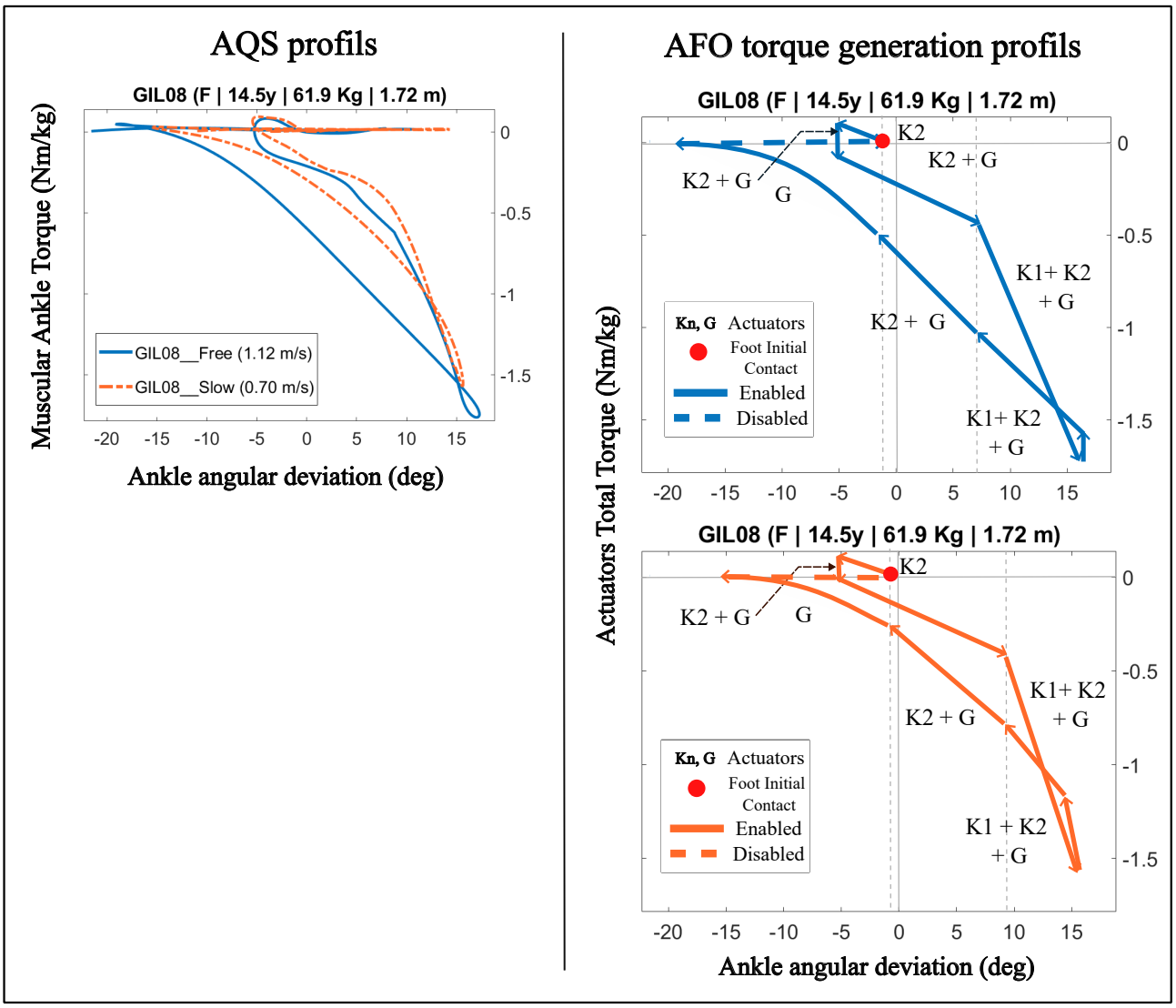

Figure A2. Fitting of the original AQS of GIL08 (female, 14.5 years old, 61.9 kg, 1.72 m) at free and slow speeds (1.12 and 0.70 m/s). GIL08 is taller than the reference GIL11 subject. Mechanism is based on linear springs (*K1*, *K2*) and an external torque generator (*G*). The starting point at left leg initial contact is pointed out by a red dot on the 2 rights curves. The AFO torque profile evolved following the arrow marks. During the swing phase (from −15° to IC clockwise), no component was enabled.

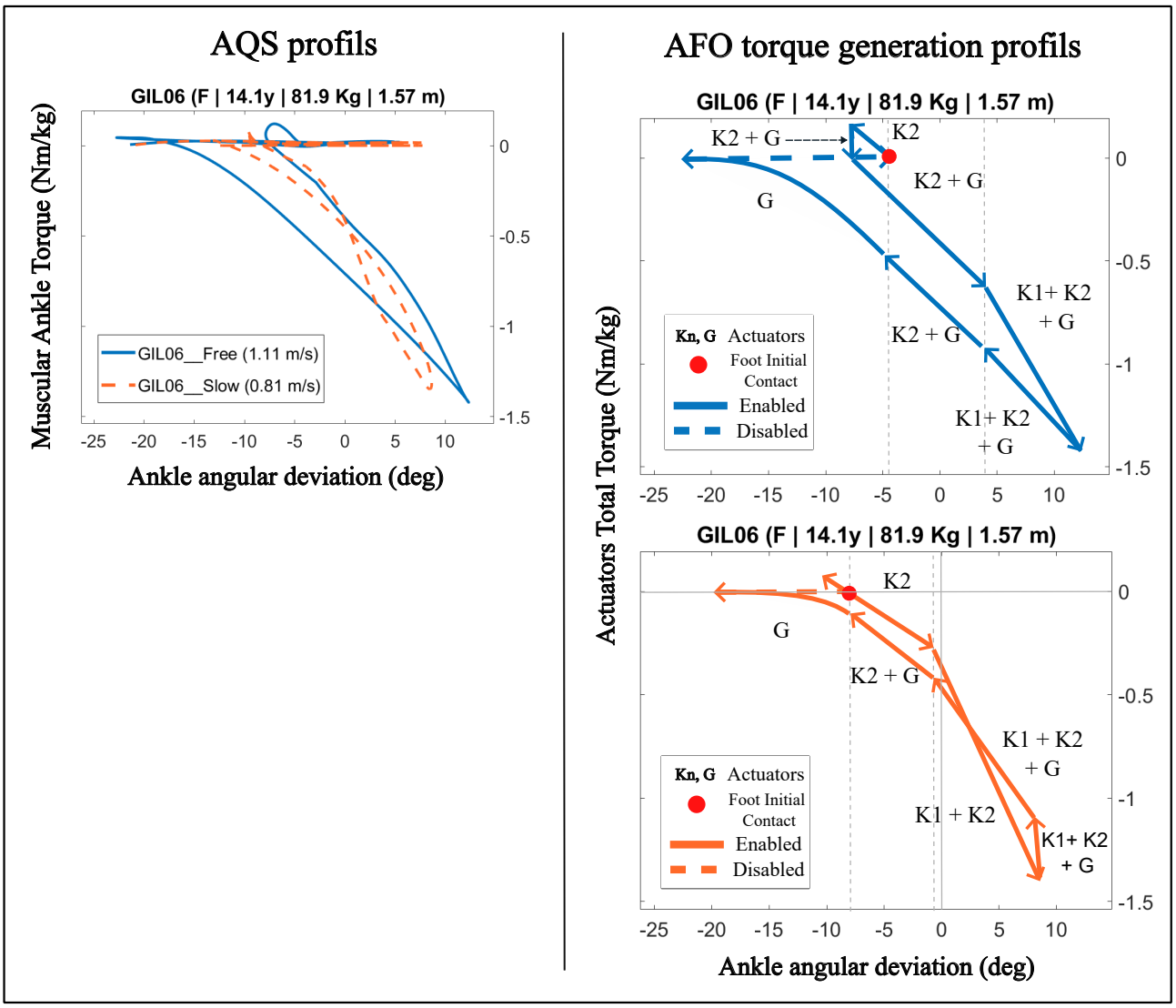

Figure A3. Fitting of the original AQS of GIL06 (female, 14.1 years old, 83.1 kg, 1.57 m) at free speed (1.17 m/s). GIL08 weighed more than the reference subject GIL11 but was the same height. Mechanism is based on linear springs (*K1*, *K2*) and an external torque generator (*G*). The starting point at left leg initial contact is pointed out by a red dot on the 2 rights curves. The AFO torque profile evolved following the arrow marks. During the swing phase (from −20° to IC clockwise), no component was enabled.

References

1. Zoss, A.; Kazerooni, H.; Chu, A. On the Mechanical Design of the Berkeley Lower Extremity Exoskeleton (BLEEX). In Proceedings of the 2005 IEEE/RSJ International Conference on Intelligent Robots and Systems, Edmonton, AB, Canada, 2–6 August 2005; pp. 3465–3472.
2. Kawamoto, H.; Lee, S.; Kanbe, S.; Sankai, Y. Power Assist Method for HAL-3 Using EMG-Based Feedback Controller. In Proceedings of the SMC '03 Conference Proceedings, 2003 IEEE International Conference on Systems, Man and Cybernetics, Conference Theme—System Security and Assurance (Cat, No.03CH37483), Washington, DC, USA, 8 October 2003; Volume 2, pp. 1648–1653.
3. Walsh, C.; Endo, K.; Herr, H. A Quasi-Passive Leg Exoskeleton for Load-Carrying Augmentation. *Int. J. Hum. Robot.* **2007**, *4*, 487–506. [CrossRef]
4. Wang, S.; Meijneke, C.; Kooij, H. Modeling, Design, and Optimization of Mindwalker Series Elastic Joint. In Proceedings of the 2013 IEEE 13th International Conference on Rehabilitation Robotics (ICORR, 2013), Seattle, WA, USA, 24–26 June 2013; pp. 1–8.
5. Human Universal Load Carrier (HULC). Available online: https://www.army-technology.com/projects/human-universal-load-carrier-hulc/ (accessed on 20 May 2024).

6. Kang, I.; Hsu, H.; Young, A. The Effect of Hip Assistance Levels on Human Energetic Cost Using Robotic Hip Exoskeletons. *IEEE Robot. Autom. Lett.* **2019**, *4*, 430–437. [CrossRef]
7. Pratt, J.; Krupp, B.; Morse, C.; Collins, S. The RoboKnee: An Exoskeleton for Enhancing Strength and Endurance during Walking. In Proceedings of the IEEE International Conference on Robotics and Automation, Proceedings ICRA, New Orleans, LA, USA, 26 April 2004; Volume 4, pp. 2430–2435.
8. Nikitczuk, J.; Weinberg, B.; Canavan, P.; Mavroidis, C. Active Knee Rehabilitation Orthotic Device With Variable Damping Characteristics Implemented via an Electrorheological Fluid. *IEEE/ASME Trans. Mechatron.* **2010**, *15*, 952–960. [CrossRef]
9. Dežman, M.; Babič, J.; Gams, A. Qualitative Assessment of a Clutch-Actuated Ankle Exoskeleton. In *Advances in Service and Industrial Robotics*; Ferraresi, C., Quaglia, G., Eds.; Springer International Publishing: Cham, Switzerland, 2018; pp. 778–786.
10. Blaya, J.; Herr, H. Adaptive Control of a Variable-Impedance Ankle-Foot Orthosis to Assist Drop-Foot Gait. *IEEE Trans. Neural Syst. Rehabil. Eng.* **2004**, *12*, 24–31. [CrossRef]
11. Russell Esposito, E.; Schmidtbauer, K.; Wilken, J. Experimental Comparisons of Passive and Powered Ankle-Foot Orthoses in Individuals with Limb Reconstruction. *J. Neuroeng. Rehabil.* **2018**, *15*, 111. [CrossRef]
12. Gordon, K.; Sawicki, G.; Ferris, D. Mechanical Performance of Artificial Pneumatic Muscles to Power an Ankle–Foot Orthosis. *J. Biomech.* **2006**, *39*, 1832–1841. [CrossRef]
13. Hamedi, M.; Salimi, P.; Aliabadi, A.; Vismeh, M. Toward Intelligent Ankle Foot Orthosis for Foot-Drop, a Review of Technologies and Possibilities. In Proceedings of the 2015 2nd International Conference on Biomedical Engineering (ICoBE, 2015), Penang, Malaysia, 30–31 March 2015; pp. 1–6.
14. Kao, P.C.; Ferris, D. Motor Adaptation during Dorsiflexion-Assisted Walking with a Powered Orthosis. *Gait Posture* **2009**, *29*, 230–236. [CrossRef]
15. Au, S.; Herr, H.; Weber, J.; Martinez-Villalpando, E. Powered Ankle-Foot Prosthesis for the Improvement of Amputee Ambulation. In Proceedings of the 2007 29th Annual International Conference of the IEEE Engineering in Medicine and Biology Society, Lyon, France, 22–26 August 2007; pp. 3020–3026.
16. Dollar, A.; Herr, H. Lower Extremity Exoskeletons and Active Orthoses: Challenges and State-of-the-Art. *IEEE Trans. Robot.* **2008**, *24*, 144–158. [CrossRef]
17. Alam, M.; Choudhury, I.; Mamat, A. Mechanism and Design Analysis of Articulated Ankle Foot Orthoses for Drop-Foot. *Sci. World J.* **2014**, *2014*, 867869. [CrossRef]
18. Cenciarini, M.; Dollar, A. Biomechanical Considerations in the Design of Lower Limb Exoskeletons. In Proceedings of the 2011 IEEE International Conference on Rehabilitation Robotics, Zurich, Switzerland, 29 June–1 July 2011; pp. 1–6.
19. Kadaba, M.; Ramakrishnan, H.; Wootten, M. Measurement of Lower Extremity Kinematics during Level Walking. *J. Orthop. Res.* **1990**, *8*, 383–392. [CrossRef]
20. Whittle, M. Clinical Gait Analysis: A Review. *Hum. Mov. Sci.* **1996**, *15*, 369–387. [CrossRef]
21. Frigo, C.; Crenna, P.; Jensen, L. Moment-Angle Relationship at Lower Limb Joints during Human Walking at Different Velocities. *J. Electromyogr. Kinesiol.* **1996**, *6*, 177–190. [CrossRef]
22. Dollar, A.; Herr, H. Active Orthoses for the Lower-Limbs: Challenges and State of the Art. In Proceedings of the 2007 IEEE 10th International Conference on Rehabilitation Robotics, Noordwijk, Netherlands, 13–15 June 2007; pp. 968–977.
23. Crenna, P.; Frigo, C. Dynamics of the Ankle Joint Analyzed through Moment–Angle Loops during Human Walking: Gender and Age Effects. *Hum. Mov. Sci.* **2011**, *30*, 1185–1198. [CrossRef] [PubMed]
24. Collins, J.; Arch, E.; Crenshaw, J.; Bernhardt, K.; Khosla, S.; Amin, S.; Kaufman, K. Net Ankle Quasi-Stiffness Is Influenced by Walking Speed but Not Age for Older Adult Women. *Gait Posture* **2018**, *62*, 311–316. [CrossRef]
25. Nalam, V.; Lee, H. Environment-Dependent Modulation of Human Ankle Stiffness and Its Implication for the Design of Lower Extremity Robots. In Proceedings of the 2018 15th International Conference on Ubiquitous Robots (UR, 2018), Honolulu, HI, USA, 26–30 June 2018; pp. 112–118.
26. Gabriel, R.; Abrantes, J.; Granata, K.; Bulas-Cruz, J.; Melo-Pinto, P.; Filipe, V. Dynamic Joint Stiffness of the Ankle during Walking: Gender-Related Differences. *Phys. Ther. Sport* **2008**, *9*, 16–24. [CrossRef] [PubMed]
27. Weiss, P.; Kearney, R.; Hunter, I. Position Dependence of Ankle Joint Dynamics—I. *Passiv. Mech. J. Biomech.* **1986**, *19*, 727–735. [CrossRef]
28. Weiss, P.; Kearney, R.; Hunter, I. Position Dependence of Ankle Joint Dynamics—II. *Act. Mech. J. Biomech.* **1986**, *19*, 737–751. [CrossRef]
29. Sobhani Tehrani, E.; Jalaleddini, K.; Kearney, R. Ankle Joint Intrinsic Dynamics Is More Complex than a Mass-Spring-Damper Model. *IEEE Trans. Neural Syst. Rehabil. Eng.* **2017**, *25*, 1568–1580. [CrossRef]
30. Shamaei, K.; Sawicki, G.; Dollar, A. Estimation of Quasi-Stiffness and Propulsive Work of the Human Ankle in the Stance Phase of Walking. *PLoS ONE* **2013**, *8*, 59935. [CrossRef]
31. Shamaei, K.; Cenciarini, M.; Dollar, A. On the Mechanics of the Ankle in the Stance Phase of the Gait. In Proceedings of the 2011 Annual International Conference of the IEEE Engineering in Medicine and Biology Society, Boston, MA, USA, 30 August–3 September 2011; pp. 8135–8140.
32. Fukuchi, C.; Fukuchi, R.; Duarte, M. Effects of Walking Speed on Gait Biomechanics in Healthy Participants: A Systematic Review and Meta-Analysis. *Syst. Rev.* **2019**, *8*, 153. [CrossRef]

33. Hansen, A.; Childress, D.; Miff, S.; Gard, S.; Mesplay, K. The Human Ankle during Walking: Implications for Design of Biomimetic Ankle Prostheses. *J. Biomech.* **2004**, *37*, 1467–1474. [CrossRef] [PubMed]
34. Mooney, L.; Rouse, E.; Herr, H. Autonomous Exoskeleton Reduces Metabolic Cost of Walking. In Proceedings of the 2014 36th Annual International Conference of the IEEE Engineering in Medicine and Biology Society, Chicago, IL, USA, 26–30 August 2014; pp. 3065–3068.
35. Sanchez-Villamañan, M.; Gonzalez-Vargas, J.; Torricelli, D.; Moreno, J.; Pons, J. Compliant Lower Limb Exoskeletons: A Comprehensive Review on Mechanical Design Principles. *J. Neuroeng. Rehabil.* **2019**, *16*, 55. [CrossRef] [PubMed]
36. Au, S.; Weber, J.; Herr, H. Powered Ankle–Foot Prosthesis Improves Walking Metabolic Economy. *IEEE Trans. Robot.* **2009**, *25*, 51–66. [CrossRef]
37. Jafari, A.; Tsagarakis, N.; Caldwell, D. AwAS-II: A New Actuator with Adjustable Stiffness Based on the Novel Principle of Adaptable Pivot Point and Variable Lever Ratio. In Proceedings of the 2011 IEEE International Conference on Robotics and Automation, Shanghai, China, 9–13 May 2011; pp. 4638–4643.
38. Baser, O.; Kizilhan, H.; Kilic, E. Mechanical Design of a Biomimetic Compliant Lower Limb Exoskeleton (BioComEx. In Proceedings of the 2016 International Conference on Autonomous Robot Systems and Competitions (ICARSC, 2016), Braganca, Portugal, 4–6 May 2016; pp. 60–65.
39. Bergmann, L.; Lück, O.; Voss, D.; Buschermöhle, P.; Liu, L.; Leonhardt, S.; Ngo, C. Lower Limb Exoskeleton With Compliant Actuators: Design, Modeling, and Human Torque Estimation. *IEEE/ASME Trans. Mechatron.* **2023**, *28*, 758–769. [CrossRef]
40. Braun, D.; Apte, S.; Adiyatov, O.; Dahiya, A.; Hogan, N. Compliant Actuation for Energy Efficient Impedance Modulation. In Proceedings of the 2016 IEEE International Conference on Robotics and Automation (ICRA, 2016), Stockholm, Sweden, 16–21 May 2016; pp. 636–641.
41. Enoch, A.; Sutas, A.; Nakaoka, S.; Vijayakumar, S. BLUE: A Bipedal Robot with Variable Stiffness and Damping. In Proceedings of the 2012 12th IEEE-RAS International Conference on Humanoid Robots, Osaka, Japan, 29 November–1 December 2012; pp. 487–494.
42. Dežman, M.; Debevec, T.; Babič, J.; Gams, A. Effects of Passive Ankle Exoskeleton on Human Energy Expenditure: Pilot Evaluation. In *Advances in Robot Design and Intelligent Control*; Rodić, A., Borangiu, T., Eds.; Springer International Publishing: Cham, Switzerland, 2017; pp. 491–498.
43. Dezman, M.; Gams, A. Pseudo-Linear Variable Lever Variable Stiffness Actuator: Design and Evaluation. In Proceedings of the 2017 IEEE International Conference on Advanced Intelligent Mechatronics (AIM), IEEE, Munich, Germany, 3–7 July 2017; pp. 785–790.
44. Bae, G.T.; Song, J.B.; Kim, B.S. Imitation of Human Motion Based on Variable Stiffness Actuator and Muscle Stiffness Sensor. In Proceedings of the 2013 IEEE/ASME International Conference on Advanced Intelligent Mechatronics, Wollongong, Australia, 9–12 July 2013; pp. 1016–1020.
45. Groothuis, S.; Rusticelli, G.; Zucchelli, A.; Stramigioli, S.; Carloni, R. The VsaUT-II: A Novel Rotational Variable Stiffness Actuator. In Proceedings of the 2012 IEEE International Conference on Robotics and Automation, Saint Paul, MN, USA, 14–18 May 2012; pp. 3355–3360.
46. Hollander, K.; Sugar, T.; Herring, D. Adjustable Robotic Tendon Using a 'Jack Spring'/Spl Trade/. In Proceedings of the 9th International Conference on Rehabilitation Robotics, 2005. ICORR 2005,Chicago, IL, USA, 28 June–1 July 2005; pp. 113–118.
47. Tsagarikis, N.; Jafari, A.; Caldwell, D. A Novel Variable Stiffness Actuator: Minimizing the Energy Requirements for the Stiffness Regulation. In Proceedings of the Annual International Conference of the IEEE Engineering in Medicine and Biology, Buenos Aires, Argentina, 31 August–4 September 2010; pp. 1275–1278.
48. Wolf, S.; Eiberger, O.; Hirzinger, G. The DLR FSJ: Energy Based Design of a Variable Stiffness Joint. In Proceedings of the 2011 IEEE International Conference on Robotics and Automation, Shanghai, China, 9–13 May 2011; pp. 5082–5089.
49. Xiong, X.; Sun, X.; Chen, W.; Zhi, Y.; Fang, X. Design of a Variable Stiffness Actuator Based on Variable Radius Mechanisms. In Proceedings of the 2022 IEEE/ASME International Conference on Advanced Intelligent Mechatronics (AIM, 2022), Royton Sapporo, Japan, 11–15 July 2022; pp. 1567–1572.
50. Yang, Z.; Guo, S. A Hybrid Motion Stiffness Control of Variable Stiffness Actuator for Upper Limb Elbow Joints Rehabilitation. In Proceedings of the 2022 IEEE International Conference on Mechatronics and Automation (ICMA, 2022), Guilin, China, 7–10 August 2022; pp. 1324–1328.
51. Zhang, L.; Huang, G.; Zhu, S.; Kong, L.; Xie, A.; Chen, L.; Zhang, D. Design of A Variable Stiffness Actuator and Study on Its Variable Stiffness Characteristics. In Proceedings of the 2022 8th International Conference on Mechanical Engineering and Automation Science (ICMEAS, 2022), Wuhan, China, 14–16 October 2022; pp. 1–6.
52. Li, Z.; Bai, S. Design and Modelling of a Compact Variable Stiffness Mechanism for Wearable Elbow Exoskeletons. In Proceedings of the 2019 7th International Conference on Control, Mechatronics and Automation (ICCMA, 2019), Delft, Netherlands, 6–8 November 2019; pp. 342–346.
53. Fu, Q.; Li, X.; Guo, J.; Guo, S.; Cai, Z.; Fu, J. Design of a Variable Stiffness Series Mechanism. In Proceedings of the 2021 IEEE International Conference on Mechatronics and Automation (ICMA, 2021), Takamatsu, Kagawa, Japan, 8–11 August 2011; pp. 909–913.
54. Wang, S.; Dijk, W.; Kooij, H. Spring Uses in Exoskeleton Actuation Design. In Proceedings of the 2011 IEEE International Conference on Rehabilitation Robotics, Zurich, Switzerland, 29 June–1 July 2011; pp. 1–6.

55. Khamar, M.; Edrisi, M.; Zahiri, M. Human-Exoskeleton Control Simulation, Kinetic and Kinematic Modeling and Parameters Extraction. *MethodsX* **2019**, *6*, 1838–1846. [CrossRef]
56. Aftabi, H.; Nasiri, R.; Ahmadabadi, M. Simulation-Based Biomechanical Assessment of Unpowered Exoskeletons for Running. *Sci. Rep.* **2021**, *11*, 11846. [CrossRef]
57. Dembia, C.; Silder, A.; Uchida, T.; Hicks, J.; Delp, S. Simulating Ideal Assistive Devices to Reduce the Metabolic Cost of Walking with Heavy Loads. *PLoS ONE* **2017**, *12*, 0180320. [CrossRef]
58. Pirjade, Y.; Londhe, D.; Patwardhan, N.; Kotkar, A.; Shelke, T.; Ohol, S. Design and Fabrication of a Low-Cost Human Body Lower Limb Exoskeleton. In Proceedings of the 2020 6th International Conference on Mechatronics and Robotics Engineering (ICMRE, 2020), Barcelona, Spain, 12–15 February 2020; pp. 32–37.
59. Liu, M.; Anderson, F.; Schwartz, M.; Delp, S. Muscle Contributions to Support and Progression over a Range of Walking Speeds. *J. Biomech.* **2008**, *41*, 3243–3252. [CrossRef]
60. Rajagopal, A.; Dembia, C.; DeMers, M.; Delp, D.; Hicks, J.; Delp, S. Full-Body Musculoskeletal Model for Muscle-Driven Simulation of Human Gait. *IEEE Trans. Biomed. Eng.* **2016**, *63*, 2068–2079. [CrossRef]
61. Github. OpenSim Gait10DOF18Muscles NMS Model. Available online: https://github.com/opensim-org/opensim-models/blob/master/Models/Gait10dof18musc/gait10dof18musc.osim (accessed on 19 May 2024).
62. Schwartz, M.; Rozumalski, A.; Trost, J. The effect of walking speed on the gait of typically developing children. *J. Biomech.* **2008**, *41*, 1639–1650. [CrossRef]
63. Thelen, D.; Anderson, F. Using computed muscle control to generate forward dynamic simulations of human walking from experimental data. *J. Biomech.* **2006**, *39*, 1107–115. [CrossRef] [PubMed]
64. Thelen, D.; Anderson, F.; Delp, S. Generating Dynamic Simulations of Movement Using Computed Muscle Control. *J. Biomech.* **2003**, *36*, 321–328,. [CrossRef] [PubMed]
65. Muller, A.; Pontonnier, C.; Puchaud, P.; Dumont, G. CusToM: A Matlab Toolbox for Musculoskeletal Simulation. *JOSS* **2019**, *4*, 927,. [CrossRef]
66. Hicks, J.; Uchida, T.; Seth, A.; Rajagopal, A.; Delp, S. Is My Model Good Enough? Best Practices for Verification and Validation of Musculoskeletal Models and Simulations of Movement. *J. Biomech. Eng.* **2015**, *137*, 020905. [CrossRef]
67. Maxon. DC Brushless Motor RE50 200W. Available online: https://www.maxongroup.fr/maxon/view/product/motor/dcmotor/re/re50/578298 (accessed on 18 August 2024).
68. Vanel tech. compression spring C-200-320-0400-i. Available online: https://www.vanel.tech/catalog/product/view/id/32659/s/c-200-320-0400-i/ (accessed on 18 August 2024).
69. Vanel tech. compression spring C-214-420-0500-i. Available online: https://www.vanel.tech/catalog/product/view/id/49123/s/c-214-420-0500-i/(accessed on 18 August 2024).
70. Vijayan, V.; Fang, S.; Reissman, T.; Kinney, A. Spatiotemporal and muscle activation adaptations during overground walking in response to lower body added mass. *Gait Posture*. **2022**, *92*, 116–122. [CrossRef]
71. Muller, A.; Pontonnier, C.; Dumont, G. Motion-Based Prediction of Hands and Feet Contact Efforts During Asymmetric Handling Tasks. *IEEE Trans. Biomed. Eng.* **2020**, *67*, 344–352. [CrossRef]
72. Kobayashi, T.; Singer, M.; Orendurff, M.; Gao, F.; Daly, W.; Foreman, K. The effect of changing plantarflexion resistive moment of an articulated ankle-foot orthosis on ankle and knee joint angles and moments while walking in patients post stroke. *Clin. Biomech.* **2015**, *30*, 775–780. [CrossRef]